Supporting Information

A polypyridyl Co(II) complex-based water reduction catalyst with double H_2 evolution sites

Junfei Wang,[a b] Chao Li,[a] Qianxiong Zhou, [a] Weibo Wang, [a] Yuanjun Hou,* [a] Baowen Zhang, [a] Xuesong Wang* [a]

[a] Key Laboratory of Photochemical Conversion and Optoelectronic Materials, Technical Institute of Physics and Chemistry, Chinese Academy of Sciences, Beijing 100190, P. R. China

[b] Graduate School of Chinese Academy of Sciences, Beijing 100049, P. R. China

Table of Contents

Materials

Cobalt (II) chloride hexahydrate, di-(2-picolyl)amine, sodium triacetoxyborohydride, 6-methyl-2-pyridinecarboxaldehyde, 2-pyridinecarboxaldehyde, 6-bromo-2-pyridine carboxaldehyde and 6-chloro-2-pyridinecarboxaldehyde were purchased from Adamas. Triethylamine (TEA) and tetrabutylammonium hexafluorophosphate were obtained from Alfa. All solvents were of analytical purity and used without further treatment. Distilled water was used in all experiments.

Determination of Faradaic Efficiency

A solution of 1 mM **1** and 20 mM acetic acid in 10 mL of Ar-saturated CH_3CN was electrolyzed at an applied potential of –2.0 V vs. SCE for 2 h in a gas-tight electrolysis cell. After electrolysis, the gas components in the headspace were analyzed by gas chromatography. The amount of hydrogen generated was determined by the external standard method and the hydrogen dissolved in the solution was neglected. The Faradaic efficiency were calculated by the equation: (the moles of H_2 evolved during the CPE process) / (the moles of H_2 calculated based on consumed charges) × 100%.

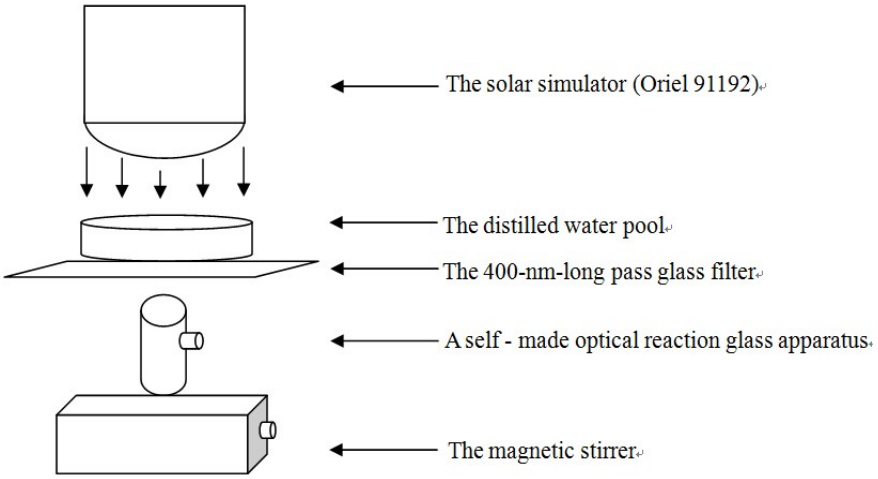

Scheme S1. Schematic presentation of the photocatalytic reaction setup.

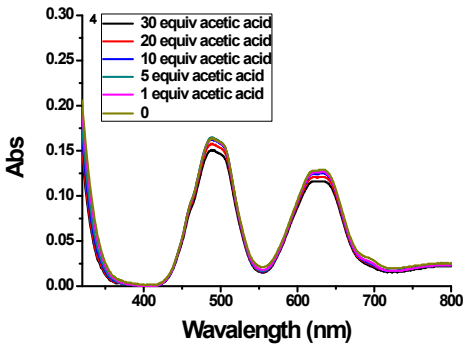

Figure S1. Absorption spectra of **4** (1 mM) in CH_3CN in the presence of various concentrations of acetic acid.

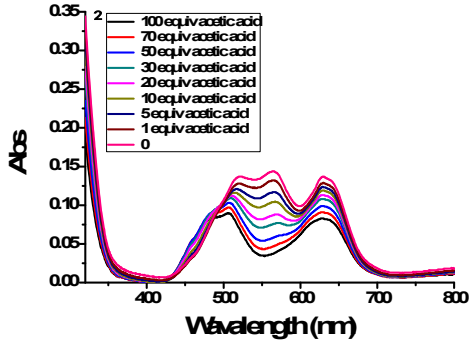

Figure S2. Absorption spectra of **2** (1 mM) in CH_3CN in the presence of various concentrations of acetic acid.

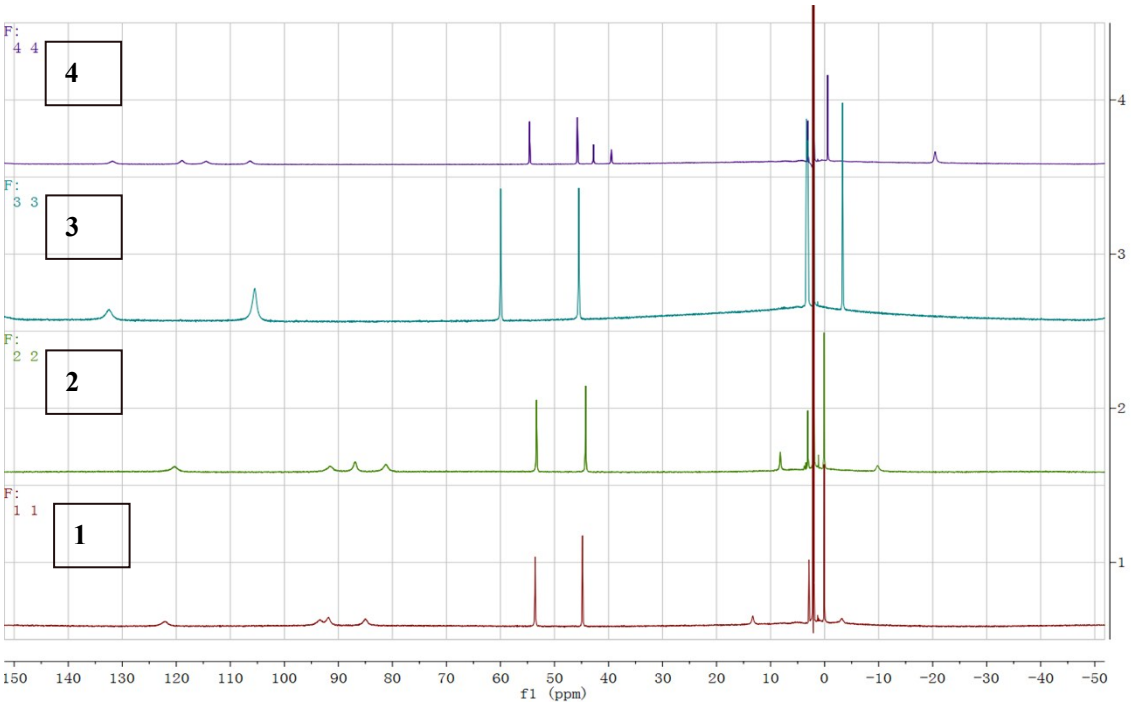

Figure S3. ^1H NMR spectra of **1-4** in CD_3CN.

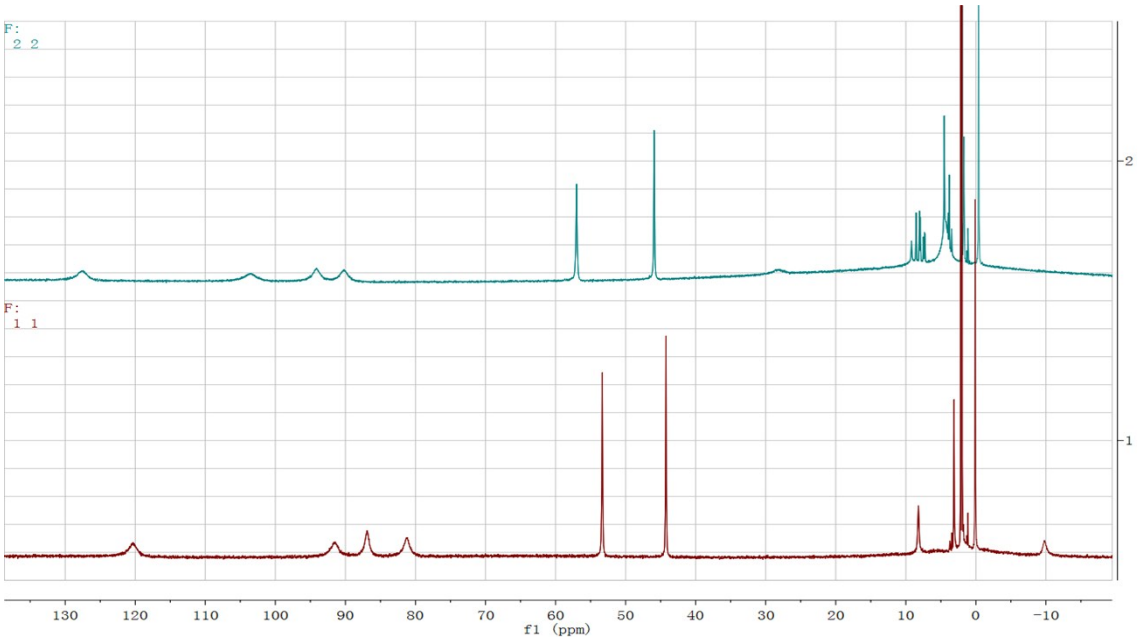

Figure S4. ^{1}H NMR of **2** (1.0 mM) in CD_3CN in the absence (bottom) or presence (top) of 1 equivalent of deuterated trifluoroacetic acid.

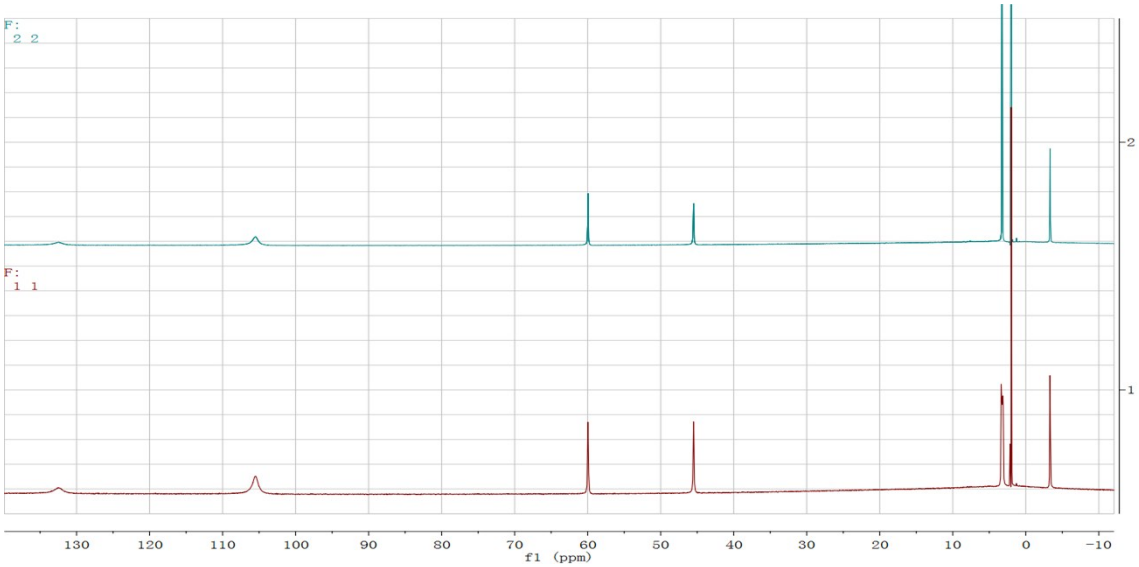

Figure S5. ^{1}H NMR of **3** (1.0 mM) in CD_3CN in the absence (bottom) or presence (top) of 1 equivalent of deuterated trifluoroacetic acid.

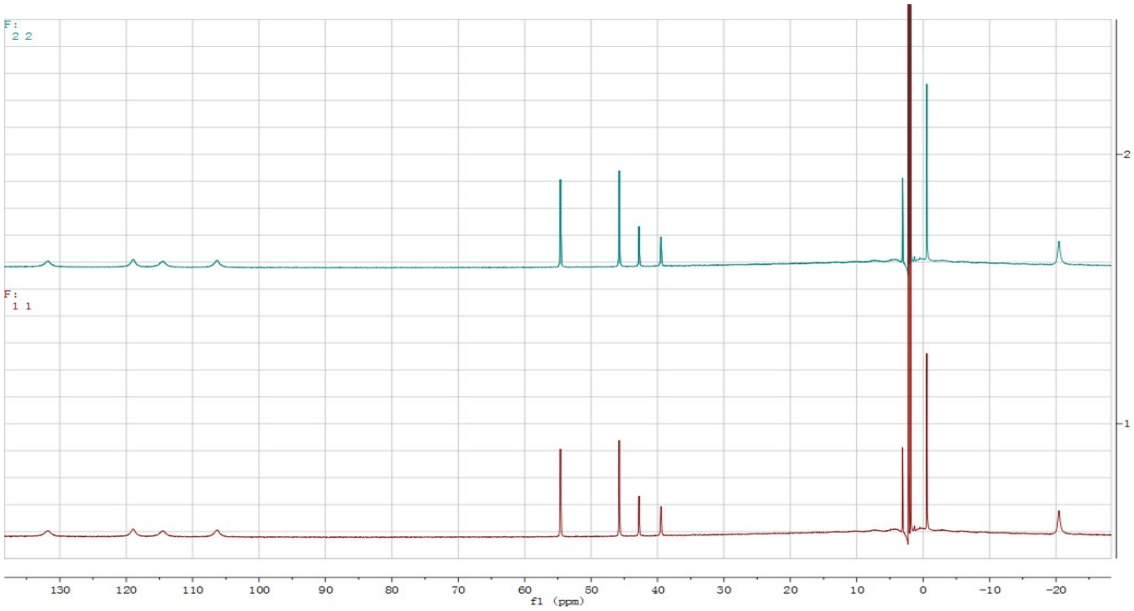

Figure S6. ^{1}H NMR of **4** (1.0 mM) in CD_3CN in the absence (bottom) or presence (top) of 1 equivalent of deuterated trifluoroacetic acid.

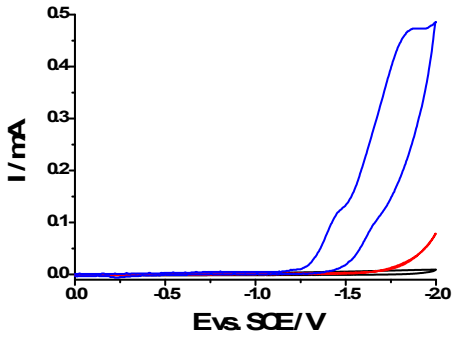

Figure S7. Cyclic voltammograms of blank CH_3CN (black), 15 mM acetic acid in CH_3CN (red), and 15 mM acetic acid and 1 mM **1** in CH_3CN (blue). Condition: 0.1 M *n*-Bu_4NPF_6, scan rate 100 mV/s.

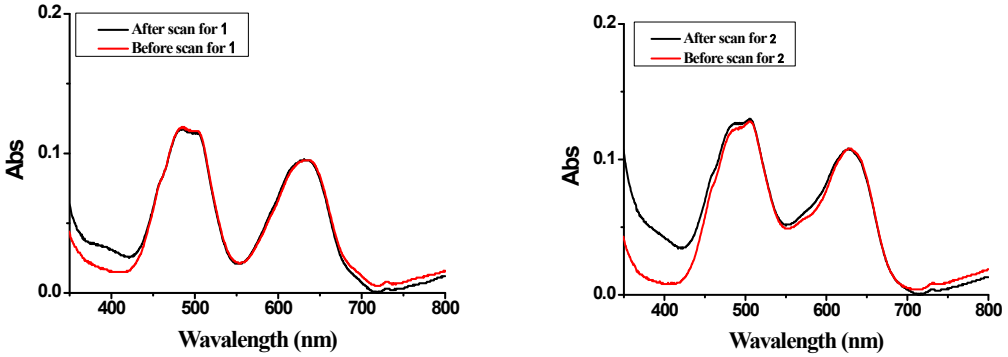

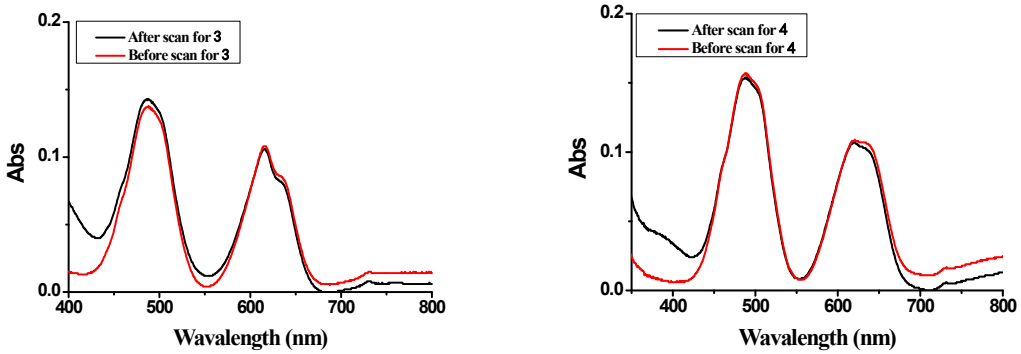

Figure S8. Absorption spectra of **1**-**4** before and after 100 cycles of CV scan in the range of 0 and -2.0 V vs SCE in Ar-saturated CH_3CN.

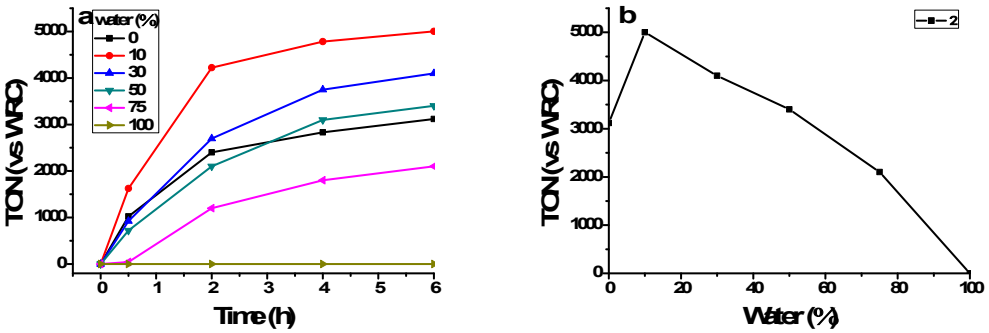

Figure S9. (a) Photocatalytic H_2 production profiles of the AP systems containing 0.1 mM $[Ir(ppy)_2(dtbpy)]Cl$, 0.01 mM **2**, 0.6 M TEA in CH_3CN/H_2O of varied compositions. (b) H_2 production amounts of the AP systems after 6 h irradiation.

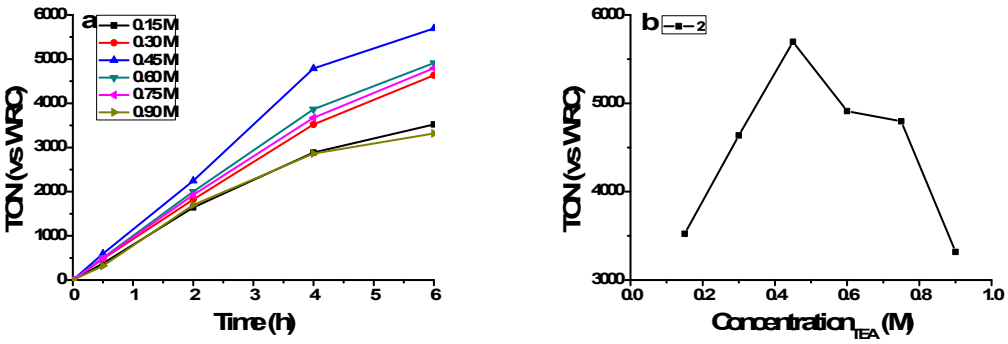

Figure S10. (a) Photocatalytic H_2 production profiles of the AP systems containing 0.1 mM $[Ir(ppy)_2(dtbpy)]Cl$, 0.01 mM **2**, and varied concentrations of TEA in CH_3CN/H_2O (9:1). (b) H_2 production amounts of the AP systems after 6 h irradiation.

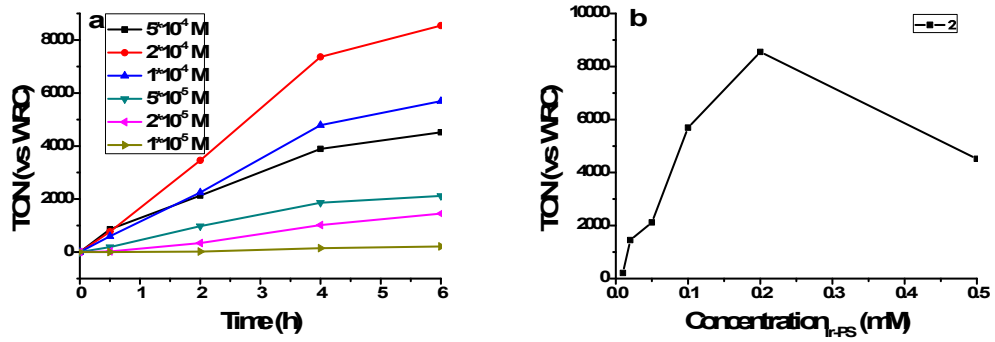

Figure S11. (a) Photocatalytic H_2 production profiles of the AP systems containing 0.01 mM **2**, 0.45 M TEA, and varied concentrations of $[Ir(ppy)_2(dtbpy)]Cl$ in CH_3CN/H_2O (9:1); (b) H_2 production amounts of the AP systems after 6 h irradiation.

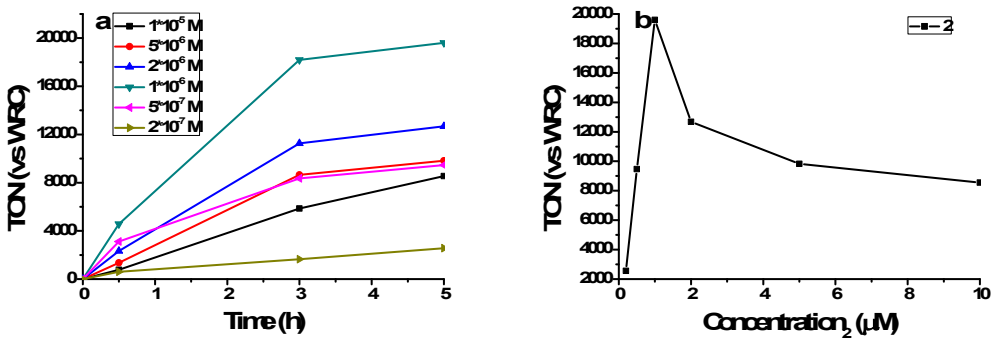

Figure S12. (a) Photocatalytic H_2 production profiles of the AP systems containing 0.2 mM $[Ir(ppy)_2(dtbpy)]Cl$, 0.45 M TEA, and varied concentrations of **2** in CH_3CN/H_2O (9:1). (b) H_2 production amounts of the AP systems after 5 h irradiation.

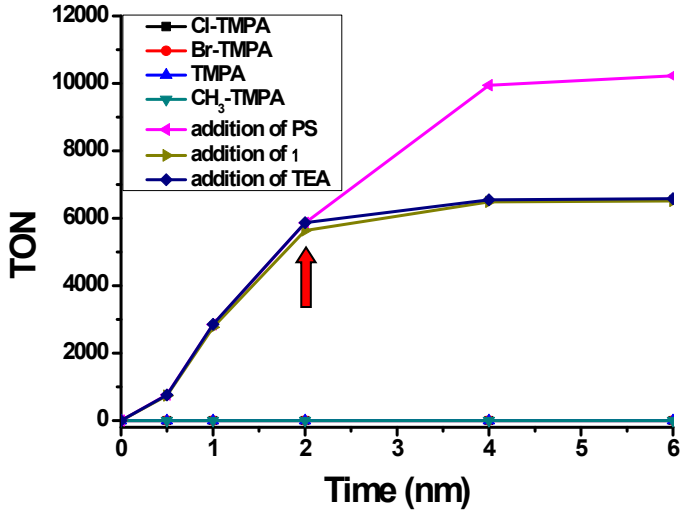

Figure 13. Photocatalytic H_2 production profiles of the AP systems containing 0.2 mM Ir-based PS, 10 μM **1** and 0.45 M TEA in Ar-saturated CH_3CN/H_2O (9:1). After 2 h of irradiation (as shown by a red arrow), 1 equiv of PS, **1**, or TEA was added, and H_2 evolution recovery was only found in the case of the addition of **1**. H_2 production profiles of the free ligands in the conditions similar to their Co complexes are also included.

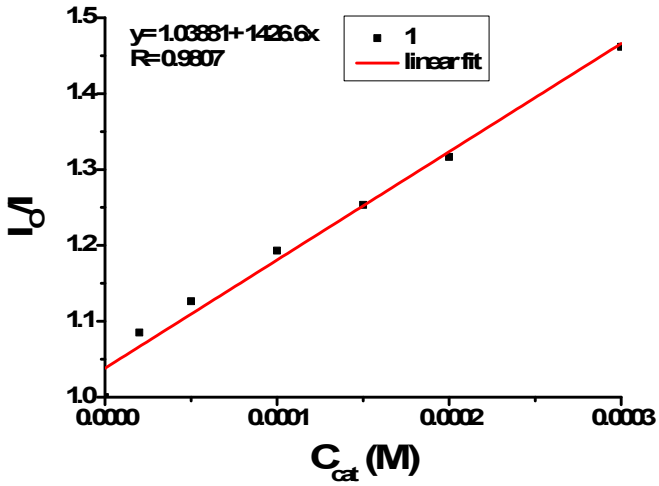

Figure S14. Stern-Volmer plot of the luminescence quenching of $[Ir(ppy)_2(dtbpy)]Cl$ by **1** in CH_3CN/H_2O (9:1).

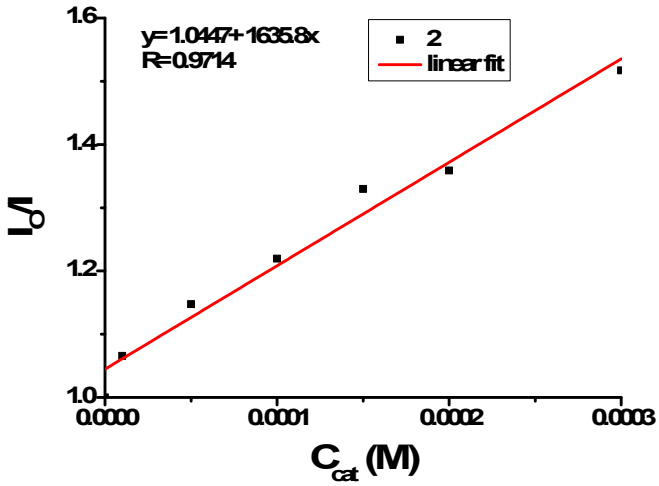

Figure S15. Stern-Volmer plot of the luminescence quenching of $[Ir(ppy)_2(dtbpy)]Cl$ by **2** in CH_3CN/H_2O (9:1).

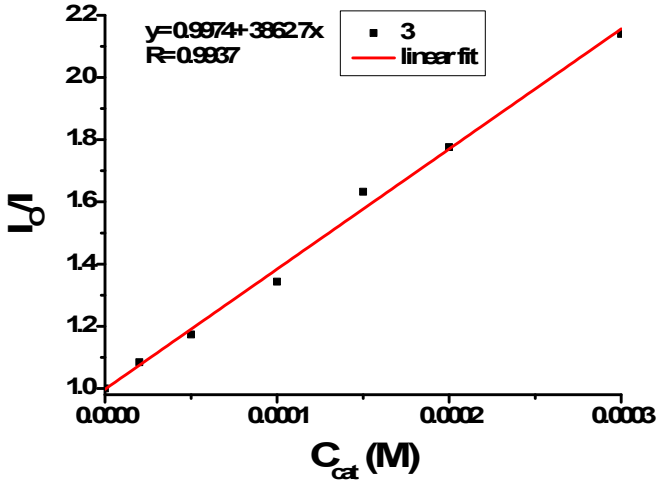

Figure S16. Stern-Volmer plot of the luminescence quenching of $[Ir(ppy)_2(dtbpy)]Cl$ by **3** in

CH_3CN/H_2O (9:1).

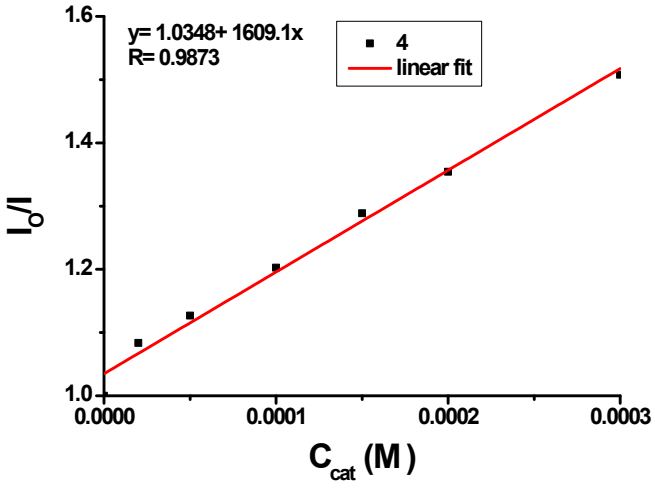

Figure S17. Stern-Volmer plot of the luminescence quenching of $[Ir(ppy)_2(dtbpy)]Cl$ by **4** in CH_3CN/H_2O (9:1).

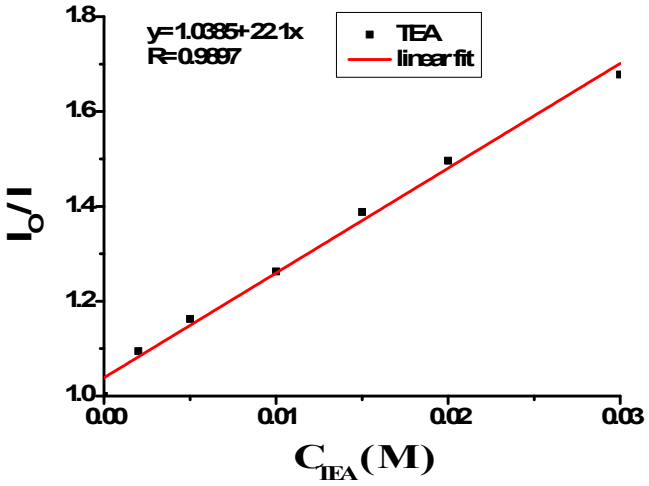

Figure S18. Stern-Volmer plot of the luminescence quenching of $[Ir(ppy)_2(dtbpy)]Cl$ by TEA in CH_3CN/H_2O (9:1).

Table S1. Selected bond lengths (Å) and angles (deg) of **2.**

Complex 2	**$[Co(Br\text{-}TMPA)Cl_2]$**
Co(1)-N(3)	**2.078(5)**
Co(1)-N(2)	**2.095(5)**
Co(1)-N(1)	**2.296(4)**
Co(1)-Cl(1)	**2.3163(16)**
Co(1)-Cl(2)	**2.3191(17)**
N(3)-Co(1)-N(2)	**110.52(17)**
N(3)-Co(1)-N(1)	**77.15(17)**
N(2)-Co(1)-N(1)	**76.60(17)**
N(3)-Co(1)-Cl(1)	**105.17(13)**
N(2)-Co(1)-Cl(1)	**135.61(13)**

N(1)-Co(1)-Cl(1)		**86.71(12)**
N(3)-Co(1)-Cl(2)	**N(2)-Co(1)-**	**100.99(14)**
Cl(2)	**N(1)-Co(1)-Cl(2)**	**96.47(13)**
Cl(1)-Co(1)-Cl(2)		**171.42(12)**
		101.84(7)

Table S2. Selected bond lengths (Å) and angles (deg) of **4.**

Complex 4		**[Co(CH_3-TMPA)Cl_2]**
Co(1)-N(3)		**2.161(3)**
Co(1)-N(2)		**2.197(3)**
Co(1)-N(1)		**2.201(4)**
Co(1)-N(4)	**Co(1)-**	**2.231(3)**
Cl(1)		**2.3719(12)**
Co(1)-Cl(2)		**2.4401(13)**
N(3)-Co(1)-N(2)	**N(3)-Co(1)-**	**82.20(12)**
N(1)		**79.07(13)**
N(2)-Co(1)-N(1)	**N(3)-Co(1)-**	**76.71(12)**
N(4)		**87.48(12)**
N(2)-Co(1)-N(4)		**152.25(13)**
N(1)-Co(1)-N(4)		**76.07(12)**
N(3)-Co(1)-Cl(1)		**92.90(10)**
N(2)-Co(1)-Cl(1)		**94.42(9)**
N(1)-Co(1)-Cl(1)	**N(4)-Co(1)-**	**168.68(8)**
Cl(1)	**N(3)-Co(1)-Cl(2)**	**111.84(10)**
N(2)-Co(1)-Cl(2)		**171.78(10)**
N(1)-Co(1)-Cl(2)		**95.57(9)**
N(4)-Co(1)-Cl(2)	**Cl(1)-Co(1)-**	**92.72(9)**
Cl(2)		**90.99(9)**
		95.16(4)

Table S3. Crystallographic data and processing parameters of **2**.

Complex	Co(Br-TMPA)Cl_2
Formula	$C_{18}H_{17}Cl_2BrCoN_4$
Formula weight	499.10
Temperature	153k
Wavelength	0.71073 Å
Crystal system, space group	Monoclinic, P2(1)/n
Unit cell dimensions	a = 14.188(7) Å alpha = 90 deg
	b = 6.883(3) Å beta = 107.131(9) deg.
	c = 21.321(11) Å gamma = 90 deg.
Volume	1989.6(16) Å^3
Z, Calculated density	4, 1.666 Kg/m^3
Absorption coefficient	3.149 mm^-1
F(000)	996

Crystal size	0.49 x 0.07 x 0.03 mm
Theta range for data collection	2.93 to 29.07 deg
Limiting indices	-16<=h<=19, -9<=k<=8, -29<=l<=29
Reflections collected / unique	16990 / 5235 [R(int) = 0.0778]
Completeness to theta = 29.07	98.2 %
Absorption correction	Semi-empirical from equivalents
Max. and min. transmission	0.9115 and 0.3076
Refinement method	Full-matrix least-squares on F^2
Data / restraints / parameters	5235 / 0 / 236
Goodness-of-fit on F^2	0.999
Final R indices [I>2sigma(I)]	R1 = 0.0832, wR2 = 0.2212
R indices (all data)	R1 = 0.1142, wR2 = 0.2478
Extinction coefficient	0.0013(10)
Largest diff. peak and hole	1.837 and -1.565 e.Å^-3

Table S4. Crystallographic data and processing parameters of **4**.

Complex	$Co(CH_3\text{-}TMPA)Cl_2$
Formula	$C_{19}H_{20}Cl_2CoN_4$
Formula weight	436.42
Temperature	293(2)k
Wavelength	0.71073 Å
Crystal system, space group	Trigonel, P3(2)21
Unit cell dimensions	a = 9.0440(16) Å alpha = 90 deg b = 9.0440(16) Å beta = 90 deg. c = 40.737(10) Å gamma = 120 deg.
Volume	2885.7(10) Å^3
Z, Calculated density	6, 1.507 Kg/m^3
Absorption coefficient	1.181 mm^-1
F(000)	1345
Crystal size	0.30 x 0.30 x 0.19 mm
Theta range for data collection	2.79 to 29.11 deg
Limiting indices	-10<=h<=12, -12<=k<=12, -55<=l<=34
Reflections collected / unique	13031 / 4738 [R(int) = 0.0475]
Completeness to theta = 29.11	95.8 %
Absorption correction	Semi-empirical from equivalents
Max. and min. transmission	0.8024 and 0.7183
Refinement method	Full-matrix least-squares on F^2
Data / restraints / parameters	4738 / 0 / 242
Goodness-of-fit on F^2	1.001
Final R indices [I>2sigma(I)]	R1 = 0.0535, wR2 = 0.1076
R indices (all data)	R1 = 0.0651, wR2 = 0.1154
Extinction coefficient	0.00(2)
Largest diff. peak and hole	0.884 and -0.394 e.Å^-3